Effects of Bath Resistance on Action Potentials in the Squid Giant Axon: Myocardial Implications

Jiashin Wu*# and John P. Wikswo, Jr.*
*The Living State Physics Group, Department of Physics and Astronomy, Vanderbilt University, Nashville, Tennessee 37235, and #Krannert Institute of Cardiology, Department of Medicine, Indiana University Medical Center, Indianapolis, Indiana 46202 USA

ABSTRACT This study presents a simplified version of the quasi-one-dimensional theory (Wu, J., E. A. Johnson, and J. M. Kootsey. 1996. A quasi-one-dimensional theory for anisotropic propagation of excitation in cardiac muscle. *Biophys. J.* 71:2427–2439) with two components of the extracellular current, along and perpendicular to the axis, and a simulation and its experimental confirmation for the giant axon of the squid. By extending the one-dimensional core conductor cable equations, this theory predicts, as confirmed by the experiment, that the shapes of the intracellular and the extracellular action potentials are related to the resistance of the bath. Such a result was previously only expected by the field theories. The correlation between the shapes of the intracellular and the extracellular potentials of the giant axon of the squid resembles that observed during the anisotropic propagation of excitation in cardiac muscle. Therefore, this study not only develops a quasi-one-dimensional theory for a squid axon, but also provides one possible factor contributing to the anisotropic propagation of action potentials in cardiac muscle.

NOMENCLATURE

1-D, 2-D, 3-D	one-dimensional, two-dimensional, three-dimensional;
AP	action potential;
ASW	artificial seawater;
c_m	specific membrane capacitance per unit axial length of the fiber (μF/cm);
θ	velocity of the steady propagation of V_m along the x axis (cm/ms);
i_{app}	the apparent membrane ionic current per unit length of fiber (μA/cm). i_{app} equals the sum of i_{ion} and the virtual membrane ionic current;
i_d	the extracellular equivalent depth current per unit axial length of fiber at the surface (μA/cm);
i_i and i_e	the intracellular and the surface equivalent extracellular axial currents (μA);
i_m and i_{ion}	the transmembrane current and the transmembrane ionic current per unit length of fiber (μA/cm);
i_{vir}	the virtual membrane ionic current per unit length of fiber (μA/cm). i_{vir} equals the difference between the quasi-1-D equation and the classical 1 -D cable equation;
r_d	the extracellular equivalent depth resistance per unit axial length of the fiber at the surface (kΩ cm);
r_i and r_e	the intracellular resistance and the surface equivalent extracellular resistance per unit length of the fiber in the axial, x, direction (kΩ/cm);
τ_i	the time constant of the foot of the intracellular potential (ms);
t	time (ms);
V_i and V_e	the intracellular and the extracellular potentials, respectively, with the reference electrode in the extracellular space far from the fiber (mV);
V_m	the transmembrane potential (mV);
x	the axis representing the direction of propagation (cm).

Received for publication 29 October1 996 and in final form 4 August 2 997.
Address reprint requests to Jiashin Wu, Ph.D., Krannert Institute of Cardiology, Dept. of Medicine, Indiana University Medical Center, 1111 West 10th Street, Indianapolis, IN 46202. Tel.: (317) 630-6270; Fax: (317) 274-9697; E-mail: wu@kimail.dmed.iupui.edu.

0006-3495/97/11/2347/12 $2.00

INTRODUCTION

The propagation of excitation in biological tissues, e.g., nerve fibers, epithelial cells, and muscle, has been described by the classical one-dimensional (l-D) core conductor cable theory (Lord Kelvin, 1855) as shown in Eq.1, and by its extensions to two- and three-dimensional spaces and also by the field descriptions of a single fiber or a bundle of fibers in bath (Clark and Plonsey, 1966, 1968; Plonsey, 1974; Andreassen and Rosenfalck, 198 1; Henriquez et al., 1988; Trayanova et al., 1990a, b; Leon and Roberge, 1990; Henriquez and Plonsey, 1990; Trayanova and Henriquez, 199 1). In 1952, Hodgkin and Huxley successfully applied the l-D theory to the propagation of excitation in the giant axon of the squid. Later, the l-D cable theory was extended to two dimensions (2-D) in an effort to describe the distribution of electrical potential in flat epithelial cells (Shiba, 197 1; Shiba and Kanno,1971), and to three dimensions (3-D) for cardiac muscle (Tung, 1979; Eisenberg et al., 1979). Tung termed the 3-D cable theory a bidomain model since it included superimposed intra- and extracellular domains.

Although the classical l-D cable theory extends to 2-D and 3-D, the l-D core conductor case remains the simplest and it has been studied extensively (Plonsey and Barr,

1988). In this model, the intracellular and the extracellular currents are limited to the axial direction only. The transmembrane potential, V_m, and the membrane ionic current, i_{ion}, are related by the classical l-D cable equation

$$\frac{1}{r_i + r_e}\frac{\partial^2 V_m(x,t)}{\partial x^2} = c_m\frac{\partial V_m(x,t)}{\partial t} + i_{ion}(x,t). \quad (1)$$

If the propagation velocity, $\theta = dx/dt$, is a constant, this equation reduces to

$$\frac{1}{(r_i + r_e)\theta^2}\frac{d^2 V_m(x,t)}{dt^2} = c_m\frac{dV_m(x,t)}{dt} + i_{ion}(x,t), \quad (2)$$

where $V_m(x,t)$ is the membrane potential, r_i and r_e are the intracellular and extracellular axial resistance per unit length of the fiber, t is the time, and c_m and i_{ion} are the membrane capacitance and membrane ionic current per unit length of the fiber. Both the intracellular potential $V_i(x,t)$ and the extracellular potential $V_e(x,t)$ in the classical l-D cable theory are proportional to the membrane potential, i.e.,

$$V_i(x,t) = \frac{r_i}{r_i + r_e}V_m(x,t),$$

and (3)

$$V_e(x,t) = -\frac{r_e}{r_i + r_e}V_m(x,t).$$

As shown by Hodgkin and Katz (1949) and by Hodgkin (1954), the shape of the action potential (AP) in uniform propagation can only be affected by the local properties of the membrane, i.e., the membrane capacitance and ionic current, not by the axial resistivity. The right-hand side of Eq. 2 is determined solely by the local membrane properties, and thus, $(r_i + r_e)\theta^2$ must be constant if the local membrane properties are uniform along the fiber. Hence, any change in axial resistivity can only result in a change of the velocity of propagation, with no effect on the shape of the AP.

This study presents a simplified version of the quasi-one-dimensional (quasi- 1 -D) theory developed for cardiac muscle (Wu et al., 1996), with two components of the extracellular current, along and perpendicular to the axis, and a simulation and its experimental confirmation for the giant axon of the squid. By extending the 1-D core conductor cable equations, this theory predicts, as confirmed by in vitro experiment, that the shapes of the intracellular and the extracellular action potentials are related to the resistance of the bath.

THE THEORY OF QUASI-l-D PROPAGATION WITH EXTRACELLULAR DEPTH CURRENT

A fundamental assumption of the classical 1-D cable theory (Eq. 1) is that the action currents associated with the propagation of excitation flow solely along the long axis of the fiber. This assumption is reasonable for the intracellular current flow in a long fiber. It represents a restricted extracellular space of a thin surface layer. For an axon in bath or for a piece of cardiac muscle, this is rarely a reasonable assumption. The field descriptions of an active fiber in bath (Clark and Plonsey, 1966, 1968; Plonsey, 1974; Henriquez et al., 1988; Trayanova, et al., 1990a, b; Leon and Roberge, 1990; Trayanova and Henriquez, 1991) replace the thin extracellular surface layer of the 1-D cable theory with a simple uniform geometry, i.e., either an unbounded or a cylindrical extracellular space. In exchange for the extracellular spatial descriptions of the potential, the field theories require much more computational resources than 1-D cable equations. The equations we present in this section preserve the efficiency of the classical 1-D cable theory with an improved description of the extracellular surface potential. They are as fast as the classical 1-D cable theory in computation without limiting the extracellular current to the axial direction, and are not associated with a particular geometry of the extracellular space.

An active fiber in a bath can be described by a simplified version of the quasi- 1 -D theory for the propagation of excitation in cardiac muscle (Wu et al., 1996), having a component of the extracellular current leaving the extracellular surface of the fiber to the bath, but without the coupling current between the fibers as in cardiac muscle. The intracellular current travels along the long axis of the fiber, $i_i(x,t)$, as in the classical 1-D theory. The extracellular current has two components: one traveling along the axis of the fiber, [the extracellular equivalent surface current, $i_e(x,t)$,] and the other departing from the surface of membrane into the extracellular space [the extracellular equivalent depth current at the surface, $i_d(x,t)$]. The extracellular depth current is defined only on the extracellular surface of the fiber acting as a current source or sink. Both $i_e(x,t)$ and $i_d(x,t)$ are the surface equivalents of the current in the bath along and at the right angle to the surface. Fig. 1 illustrates the current pathways. Since we do not define the extracellular space outside the surface of the fiber, this theory is not limited to any specific extracellular space, e.g., a uniform unbounded bath, or a cylindrical bath, such as in the field theories.

The axial voltage gradients and currents obey Ohm's law, i.e.,

$$\frac{\partial V_i(x,t)}{\partial x} = -i_i r_i(x,t) \quad (4)$$

$$\frac{\partial V_e(x,t)}{\partial x} = -i_e r_e(x,t), \quad (5)$$

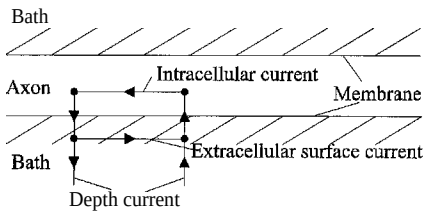

FIGURE 1 The currents in the quasi-l-D cable theory for the giant axon of a squid in a bath. The intracellular current flows inside the axon along the axis. The extracellular current has two components: the extracellular surface current (along the axis) and the extracellular depth current (perpendicular to the axis).

where x represents the spatial variable along the fiber, and $V_i(x,t)$ and $V_e(x,t)$ are the intracellular and the extracellular potentials, both with respect to a distant point outside the fiber and at zero potential.

The axial change in the intracellular axial current equals the transmembrane current. The change in extracellular axial current equals the sum of the transmembrane current, i_m, and the extracellular equivalent depth current at the surface, i_d, so that

$$\frac{\partial i_i(x,t)}{\partial x} = -i_m(x,t) \tag{6}$$

$$\frac{\partial i_e(x,t)}{\partial x} = i_m(x,t) - i_d(x,t). \tag{7}$$

We differentiate Eq. 4 and combine it with Eq. 6 to obtain

$$\frac{\partial^2 V_i(x,t)}{\partial x^2} r = i_m(x,t). \tag{8}$$

Similarly, Eqs. 5 and 7 yield

$$\frac{\partial^2 V_e(x,t)}{\partial x^2} = (i_d(x,t) - i_m(x,t))r_e. \tag{9}$$

By using the definition of the transmembrane potential,

$$V_m(x,t) = V_i(x,t) - V_e(x,t), \tag{10}$$

and subtracting Eq. 9 from Eq. 8, we obtain

$$\frac{\partial^2 V_m(x,t)}{\partial x^2} = (r_i + r_e) i_m(x,t) - r_e i_d(x,t). \tag{11}$$

The transmembrane current, $i_m(x,t)$, is the sum of the membrane capacitive current and the membrane ionic current, $i_{ion}(x,t)$, i.e.,

$$i_m(x,t) = c_m \frac{\partial V_m(x,t)}{\partial t} + i_{ion}(x,t). \tag{12}$$

By substituting this into Eqs. 8 and 11, we obtain

$$\frac{1}{r_i}\frac{\partial^2 V_i(x,t)}{\partial x^2} = c_m \frac{\partial V_i(x,t)}{\partial t} + i_{ion}(x,t) - c_m \frac{\partial V_e(x,t)}{\partial t} \tag{13}$$

and

$$\frac{1}{r_i + r_e}\frac{\partial^2 V_m(x,t)}{\partial x^2} = c_m \frac{\partial V_m(x,t)}{\partial t} + i_{ion}(x,t) - \frac{r_e}{r_i + r_e} i_d(x,t). \tag{14}$$

Both Eqs. 13 and 14 are similar to the 1 -D cable equation (Eq. 1), except one extra term is added to the membrane ionic current. When steady propagation of an AP is established along the fiber, the velocity of propagation along the fiber axis, $\theta = dx/dt$, is constant. Therefore, we can eliminate the spatial derivative and change Eq. 14 into an ordinary differential equation

$$\frac{1}{(r_i + r_e)\theta^2}\frac{d^2 V_m(x,t)}{dt^2} = c_m \frac{dV_m(x,t)}{dt} + i_{ion}(x,t) - \frac{r_e}{r_i + r_e} i_d(x,t). \tag{15}$$

Similar to the quasi-l-D theory for cardiac muscle (Wu et al., 1996), a virtual membrane current, $i_{vir}(x,t)$, is defined as the extra term in Eq. 15 in addition to the cable equation (Eq. 2), and an apparent membrane ionic current, $i_{app}(x,t)$, is defined as the sum of the membrane ionic and the virtual currents. Then we have

$$i_{vir}(x,t) = -\frac{r_e}{r_i + r_e} i_d(x,t)$$

and

$$i_{app}(x,t) = i_{ion}(x,t) + i_{vir}(x,t), \tag{16}$$

which allow us to rewrite Eqs. 14 and 15 as

$$\frac{1}{r_i + r_e}\frac{\partial^2 V_m(x,t)}{\partial x^2} = c_m \frac{\partial V_m(x,t)}{\partial t} + i_{app}(x,t) \tag{17}$$

and

$$\frac{1}{(r_i + r_e)\theta^2}\frac{d^2 V_m(x,t)}{dt^2} = c_m \frac{dV_m(x,t)}{dt} + i_{app}(x,t). \tag{18}$$

Equations 17 and 18 are in the same forms as the classical l-D cable equations (Eqs. 1 and 2), except that the apparent membrane ionic currents in Eqs. 17 and 18 are used instead of the original transmembrane ionic current in Eqs. 1 and 2. In this way, all the theoretical analysis developed for cable equations 1 and 2 can be adopted to the quasi-l-D cable theory with a simple replacement of $i_{ion}(x,t)$ with $i_{app}(x,t)$.

Combining Eqs. 8 and 12, and then using the derivative of Eq. 10 to eliminate $V_i(x,t)$, we get

$$\frac{1}{r_i}\frac{\partial^2 V_m(x,t)}{\partial x^2} = c_m \frac{\partial V_m(x,t)}{\partial t} + i_{ion}(x,t) - \frac{1}{r_i}\frac{\partial^2 V_e(x,t)}{\partial x^2}. \tag{19}$$

Subtracting Eq. 14 from Eq. 19, we have

$$i_d(x,t) = \frac{1}{r_i}\frac{\partial^2 V_m(x,t)}{\partial x^2} + \left(\frac{1}{r_i} + \frac{1}{r_e}\right)\frac{\partial^2 V_e(x,t)}{\partial x^2}. \tag{20}$$

Using Eq. 10, we can convert Eq. 20 to

$$\frac{\partial^2 V_m(x,t)}{\partial x^2} = \left(1 + \frac{r_e}{r_i}\right)\frac{\partial^2 V_i(x,t)}{\partial x^2} - r_e i_d(x,t) \tag{21}$$

and

$$\frac{\partial^2 V_e(x,t)}{\partial x^2} = \frac{r_e}{r_i}\frac{\partial^2 V_i(x,t)}{\partial x^2} + r_e i_d(x,t). \tag{22}$$

Equations 21 and 22 show the relationships between $V_m(x,t)$ and $V_i(x,t)$ and between $V_i(x,t)$ and $V_e(x,t)$. When

the magnitude of $i_d(x,t)$ is non-zero, $V_m(x,t), V_i(x,t)$, and $V_e(x,t)$ are no longer related to each other linearly, in contrast to the linear relationships of the classical l-D cable theory (Eq. 3).

Since both $V_e(x,t)$ and $i_d(x,t)$ are only defined along the axis, it is useful to define an extracellular equivalent depth resistance per unit length of fiber at the surface, r_d, as the ratio of the extracellular surface potential, V_e, and the extracellular equivalent depth current per unit length of fiber at the surface, i_d,

$$r_d(x,t) = \frac{V_e(x,t)}{i_d(x,t)}. \tag{23}$$

Just as we had with $V_e(x,t)$ and $i_d(x,t), r_d(x,t)$ is only defined on the extracellular surface of the axon. Substituting Eq. 23 into Eq. 20, we find that

$$\frac{V_e(x,t)}{r_d(x,t)} = -\frac{1}{r_i}\frac{\partial^2 V_m(x,t)}{\partial x^2} + \left(\frac{1}{r_i}+\frac{1}{r_e}\right)\frac{\partial^2 V_e(x,t)}{\partial x^2}. \tag{24}$$

With steady propagation, we have

$$\frac{\theta^2}{r_d(x,t)} V_e(x,t) = \frac{1}{r_i}\frac{\partial^2 V_m(x,t)}{\partial t^2} + \left(\frac{1}{r_i}+\frac{1}{r_e}\right)\frac{\partial^2 V_e(x,t)}{\partial t^2}. \tag{25}$$

Equation 25 shows the relationships among $V_e, \partial^2 V_m/\partial t^2$, and $\partial^2 V_e/\partial t^2$. Depending on the tissue resistivity, Eq. 25 can be simplified to

$$\frac{\theta^2}{r_d(x,t)} V_e(x,t) = \frac{1}{r_i}\frac{\partial^2 V_m(x,t)}{\partial t^2}$$

for (26)

$$\frac{\theta^2}{r_d(x,t)} V_e(x,t) \gg \left(\frac{1}{r_i}+\frac{1}{r_e}\right)\frac{\partial^2 V_e(x,t)}{\partial t^2},$$

or

$$\frac{1}{r_i}\frac{\partial^2 V_m(x,t)}{\partial t^2} = -\left(\frac{1}{r_i}+\frac{1}{r_e}\right)\frac{\partial^2 V_e(x,t)}{\partial t^2}$$

for (27)

$$\frac{\theta^2}{r_d(x,t)} V_e(x,t) \ll \left(\frac{1}{r_i}+\frac{1}{r_e}\right)\frac{\partial^2 V_e(x,t)}{\partial t^2}.$$

In the extreme cases, the shape of the extracellular potential V_e can approach either the shape of $\partial^2 V_m/\partial t^2$ (Eq. 26) or the shape of V_m (Eq. 27). In the limit of Eq. 27, V_e and V_m are proportional. Therefore, the extreme case of Eq. 27 is similar to the classical 1 -D cable theory as shown in Eq. 3. The extreme case of Eq. 26 is similar to Plonsey's expression for V_e on the membrane surface when the thickness of the stack of single-layer disk sources of current approaches zero. Using the field theory, Plonsey (1974) demonstrated that for an active fiber in an infinite bath, V_e can be described in terms of the potential from a stack of single-layer disk sources of current. Each disk has a strength approximately proportional to $\partial^2 V_m/\partial t^2$. The potential at a point in the bath is proportional to the integral of the strength of each disk divided by the distance between the disk and the point. Plonsey showed that the shape of the extracellular potential was similar to $\partial^2 V_m/\partial t^2$, with some small differences resulting from the smoothing effect of the integral. When the thickness of the stack of disk sources is reduced, so is the smoothing effect. In the general case of Eq. 25, V_e is a composition of both $\partial^2 V_m/\partial t^2$ and V_m in different proportions. Equation 25 is in good agreement with the results of the simulations based on the field theory (Trayanova et al., 1990a) for an active fiber in a restricted co-axial volume conductor. Trayanova et al. showed that the waveform of the extracellular surface potential of an active fiber in a restricted volume conductor depended on the thickness of the co-axial volume conductor. For the radius of a volume conductor, b, that is larger than 25 times the radius of the active fiber, a, the shape of V_e is biphasic or triphasic, similar to $\partial^2 V_m/\partial t^2$. For $b \leq 3a$, the shape of V_e is similar to V_m. For b intermediate between 3a and $25a$, the shape of V_e is similar to the combination of $\partial^2 V_m/\partial t^2$ and V_m in different proportions.

THE METHODS OF EXPERIMENT AND SIMULATION

Quasi-l-D propagation in the giant axon of squid

We conducted the experiments on the giant axons (stellar nerve) of the squid *Loligo pealei* to demonstrate that the shape of the propagating AP could be altered by changing the depth of the extracellular bath. We used a 100-mm diameter glass dish with its interior bottom coated with a thick flat layer of Sylgard (Dow Corning, Midland, MI) to hold the artificial sea water (ASW), the axon, and the electrodes (see Fig. 2). The ASW was composed of 430 mM NaCl, 10 mM KCl, 50 mM $MgCl_2$, 10 mM $CaCl_2$, and 10 mM HEPES, and was adjusted to pH 7.4 at room temperature and bubbled with air. We adjusted the level of ASW in the dish by either filling it with fresh ASW or removing excess ASW with a hand-held tube connected to a suction pump.

Since we were interested in seeing the effects of changing bath resistance on the AP while holding extracellular ion concentrations constant, the safest and the most reliable way was to change the height of the bath. The effective resistance of the bath at different heights of ASW was measured

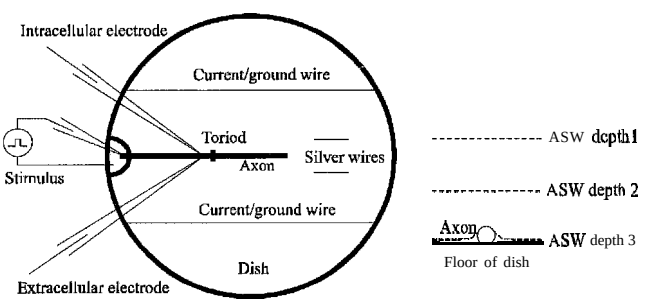

FIGURE 2 The axon and the electrodes in the dish. The two long wires at both sides of the axon serve as the ground wires during the recording of the activation and as the outer current wires when measuring the resistance of the bath with the 4-electrode method. The toroid is used to measure the intracellular axial current. The two short silver wires detect the potential for determining the resistance of the bath. The depth of the ASW is the control variable as shown in the diagram at right.

with the 4-electrode method using a pair of outer linear electrodes for current injection and a second pair of inner electrodes for voltage measurement. The effective resistance of the bath is the resistance between two parallel sides of a square of the bath in the dish. It has the units of Ω, and is inversely proportional to the height of ASW. As shown in Fig. 2, the pair of outer electrodes consisted of two 70-mm-long AgCl-coated parallel silver wires with 18-mm separation that spanned wall-to-wall the Sylgard floor of the dish. They also served as the ground electrodes during the recordings of the activation in the axons. A 50–60-Hz sine wave current (generated by the function generator, model 180LF, Wavetek, San Diego, CA) was injected into the ASW through the pair of outer electrodes. A second pair of parallel electrodes (silver wires with 4-mm separation and -5 mm in length, located within and parallel to the pair of outer electrodes) measured the voltage drop in the ASW between the electrodes. A 326 Ω resistor was in series with the pair of outer current electrodes to limit and measure the current. Two channels on an oscilloscope (Model DRO 2608, Gould, Ilford, Essex, UK) monitored the voltage across the resistor and also across the pair of inner electrodes. The resistance of the ASW was calculated from the measured voltage drops across the pair of inner electrodes and across the resistor. The axon was placed along a parallel line centered between the outer electrodes, i.e., 9 mm away from either one of the outer electrodes.

A suction stimulation electrode was applied to the surface of the axon near one end. The suction electrode was made out of glass pipette and connected electrically to a stimulator (model 850A, W-P Instruments, Inc., New Haven, CT) and physically to a syringe to provide the suction. Both the suction electrode and a stimulation ground wire were placed in a well cut in the Sylgard floor next to the wall of the dish. This well was designed to keep the stimulation electrodes and a short section of axon submerged in the bath in order to provide reliable stimulation even when the bath for the rest of the axon was reduced to a thin film. Two glass microelectrodes with their amplifier (Axoclamp-2B, with HS-2A head stage, Axon Instruments, USA) were used to record the intra and the extracellular potentials in the axons. The giant axons were pinned to the floor of the dish after being dissected from the squid. A 5-10 mm section on each axon was cleaned to facilitate the impalement of the intracellular microelectrode. After each impalement, the tip of the intracellular electrode was positioned near the axis of the axon. The tip of the extracellular microelectrode was positioned next to the membrane of the axon at a site as close to the tip of the intracellular microelectrode as possible along the axon. The axial distance between the tips of the intracellular and the extracellular electrodes was kept to less than one-tenth of the diameter of the axon (of -200-400 μm). A toroidal pick-up coil (1 mm inner diameter) with its amplifier (Neuromagnetic Current Probe, Living State Physics Group, Vanderbilt University, Nashville, TN) for measuring the intracellular axial action current (Wikswo et al., 1983; Wikswo and van Egeraat, 1991; van Egeraat and Wikswo, 1993) was placed -6 mm from the microelectrodes. The amplified signals of the intracellular and extracellular potentials and the action current were recorded with a Macintosh IIci computer equipped with an A/D converter and the LabVIEW software (National Instrument, Austin, TX) at a rate of 50K samples per second per channel. Since the intracellular axial action current was relatively noisy, we averaged the waveforms to reduce the noise. For consistency in the data handling, we also averaged the intracellular and the extracellular potentials at the same time, although both had an adequate signal-to-noise ratio before the averaging. While the signal-to-noise ratio of the intracellular axial action current improved greatly after the averaging, the potential signals showed little change.

The height of ASW in the dish was reduced in several steps on each axon from -5 mm to a thin film maintained by the surface tension of ASW. At each ASW step, we measured and recorded the resistance of the bath first, then stimulated the axon 32 times at the rate of 2/s and recorded 8 ms of the averaged signals of the intracellular potential, the extracellular potential, and the axial current. The dish was refilled with fresh ASW after the bath level was reduced to the minimum. Then another round of recording was repeated until the axon response began to degrade. Due to the difficulty in controlling the height of ASW when it was reduced to a thin layer, we did not attempt to repeat each series of the recordings at the same heights of ASW.

The simulation model and its parameters

We built a simulation model to compare the theory and experiments. Since the equations we presented were new and more abstract in defining the extracellular current than the experiments, we designed the simulation model to resemble the experiments. Although the extracellular current in the theory is represented by only two components, one along the axis of the axon and the other perpendicular to the surface of the axon into the bath, the bath in the simulation has more details. The equations derived above will be used to explain the results of the experiments and the simulations. As shown in Fig. 3, the intracellular space is represented by a single line of interconnected resistors, r_i. The bath is represented by a mesh of the extracellular resistors, r_{dl}, parallel to the axon, and r_{dt}, perpendicular to the axon. One side of the bath connects to the membrane of the axon, and the other side of the bath connects to the ground. Both r_{dl} and r_{dt} are calculated from the bath resistivity, the height of the bath, and the length and the width of the bath element. The detailed bath is compatible with the quasi-l-D equations, since the extracellular surface current can still be separated into the same two components. The intra and extracellular spaces are separated by the cell membrane, which is composed of membrane capacitance and transmembrane Na^+, K^+, and leakage currents.

Table 1 contains the parameters used in the simulation. Hodgkin-Huxley (1952) kinetics of membrane Na^+ and K^+ currents of the giant axon of the squid are used. There are 1000 100-μm-long elements in the axon, giving a total length of 100 mm. One hundred 400-μm-wide interconnected rows of elements parallel to the axon comprise the mash of the extracellular bath. The length of the elements, 100 μm, is chosen to be <1/5 of the length constant of the fully activated membrane of 550 μm. This ratio of discretization to the length constant of the fully activated membrane is small enough to avoid any significant discretization error in the continuous model. The number and the size of the elements in each bath row are the same as in the axon. Therefore, each bath element is 0.1 by 0.4 mm, along and transverse to the axon, respectively. A stimulus, 0.5 ms in duration and 12 μA in amplitude, is applied to the first intracellular element of the fiber at the starting time. The Crank-Nicolson partial differential equation solver is used to solve the propagation of the transmembrane potential with a time step, Δt, of 0.05 μs. The mesh ratio, $\Delta t/(r_i c_m \Delta x^2)$, in the model is 0.083, less than the upper limit of 1 .O (Plonsey and Barr, 1988), thereby maintaining the accuracy and the stability of the computation. The height, and hence the resistance, of the bath is the primary variable for the simulation runs. The simulation model is written in the C language and runs on various SunSparc Stations.

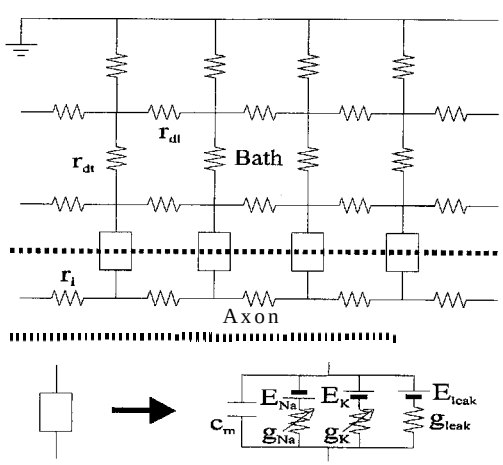

FIGURE 3 The partial structure of the simulation model of an axon in bath. r_i is the intracellular resistance; r_d is the extracellular depth resistance; c_m is the membrane capacitance. g_{Na}, g_K, g_{leak}, E_{Na}, E_K, and E_{leak} are the Na^+, K^+, and leakage conductances, and the Na^+, K^+, and leak equilibrium potentials, respectively. In the simulation, the axon and bath are 1000 elements long and the bath is 100 elements wide.

TABLE 1 The parameters used in the simulation models

Specific membrane capacitance C_m	1.0 μF/cm^2
Maximum membrane Na^+ conductivity, $\bar{g}_{Na}$	120 mS/cm^2
Maximum membrane K^+ conductivity, $\bar{g}_K$	36 mS/cm^2
Membrane leakage conductivity, g_{leak}	0.3 mS/cm^2
Intracellular Na^+ concentration	59 mM
Extracellular Na^+ concentration	430 mM
Intracellular K^+ concentration	207 mM
Extracellular K^+ concentration	10 mM
Intracellular Cl^- concentration	65 mM
Extracellular Cl^- concentration	560 mM
Temperature	22°C
Temperature factor for the gating process of channels	3.0 per 10°C
Temperature factor for the ionic currents	1.3 per 10°C
Specific intracellular axial resistivity	60 Ω cm
Resistivity of the bath	20 Ω cm
Diameter of the axon	0.4 mm

RESULTS

The resistance per surface area of the bath is the primary variable in both of the experiments and the simulations. Since the height of ASW is much smaller than the length of the axon or the diameter of the dish, the current distribution in the bath is basically two-dimensional, on the bottom of the dish. The resistance per surface unit of the bath is inversely proportional to the height of the bath, and is adjusted by changing the height of the bath in the experiments. During the experiments, the resistance per surface area of the bath was measured between two parallel silver electrodes in the bath. Since we only cleaned a section of axon ~5–10 mm long free of the surface filaments to minimize the possible damage of cleaning to the axon, the thin layer of the bath surrounding the axon could be uneven when the bath was reduced to less than the thickness of the surface filaments at the lowest level. Except with the lowest level of ASW, the recorded extracellular potentials are reliable. Due to the surface tension of the ASW around the axon, there might be more ASW around the axon than the measured bath resistance called for. In the simulations, the resistance per surface area of the bath is calculated from the height of the bath and the bath resistivity.

All experimental data presented here are from the axons with higher than 100 mV amplitude of the intracellular potential (Adelman and Gilbert, 1990) at high ASW level and with <0.3 mV difference between the amplitudes of the intracellular APs at the beginning and after the end of a series of recording when the bath was refilled to the initial level. The membrane potential, V_m, is derived from the difference between the intracellular and the extracellular potential recordings, which are relative to their resting states. The maximum rates of rising of V_i and V_m are the peak values of $\Delta V_i/\Delta t$ and $\Delta V_m/\Delta t$, where At is the sampling interval, 0.02 ms. The time constants of the feet of V_i and V_m are the lowest values calculated from three samples at 0.08-ms intervals at the foot of AP. The simulation results are obtained from the middle point of the axon to minimize the boundary and stimulus artifacts which are limited mostly to the first and the last 100 elements of the model of axon. In the simulations, the At for the rate of change of V_i and V_m is 0.05 μs, and the time interval of the three samples for calculating the time constants of the feet of V_i and V_m is 0.15 μs.

As shown in Fig. 4, the waveforms and the phase plots of the typical experimental data are similar to their corresponding simulations. Since the bath resistance in the simulation can be set to any value, we used 16 Ω and 1000 Ω, for the high and the low ASW levels, to clearly demonstrate the differences in their effects on the waveforms of AP. These values of the bath resistance are more extreme than the experimentally measured values of 108 Ω and 445 Ω for the high and the low ASW levels. The 16 Ω bath resistance used in simulation results in a much smaller amplitude of the extracellular potential (Fig. 4 *f*) than that experimentally recorded at high ASW. Therefore, the high ASW simulation is similar to the expections of the classical l-D cable theory (Eq. 1) with a grounded extracellular space.

Figure 5 shows the effects of the bath resistance on the characteristic parameters of the waveforms of the intracellular and the membrane APs (the time constant of the foot, the amplitude, and the maximum rate of rise), on the peak-to-peak amplitude of the extracellular potential, and on the axial currents of the five experimental recordings from three axons. Due to the uncontrolled factors, e.g., the geometrical sizes of axons, the differences in the cleanliness of their surfaces, etc., the recorded data differ from axon to axon, although the similar responses to the bath resistance exist in all recordings. The corresponding results of the simulation are in Figs. 6 and 7 *i*. The comparison of the experimental data and the simulation results are presented in Fig. 7. Except for plots *d* and *i*, all other plots in Fig. 7 are derived from Figs. 5 and 6. To combine the experimental data from different axons and to facilitate the comparison with the simulated results, each set of the data in Fig. 5 is normalized by dividing the data of each recording with either the values at the highest level of ASW (*a–c*) or its mean (*e*). Therefore, the initial differences among the five recording series arising from axon-to-axon variation are removed. Then the normalized data from the five recording series are combined and presented in the upper panel of Fig. 7. Due to the difficulty in controlling the height of ASW precisely at low level, the values of the bath resistance at which the data are measured vary between axons. Consequently, we fit the data with the least-square lines and their 95% confidence boundaries (the thin dashed lines on both sides of the thick least-square lines). The least-square lines and their 95% confidence boundaries are equivalent to the conventional statistical representations. As shown in Fig. 7, *a–e*, the 95% confidence boundaries have very limited overlays between the data of the V_i and the V_m, indicating the significant differences between them. Plots&/z, and *j*, in Fig. 7 are the normalized simulation results derived from Fig. 6. The behavior of the simulated results closely resembles that of the experimental observations.

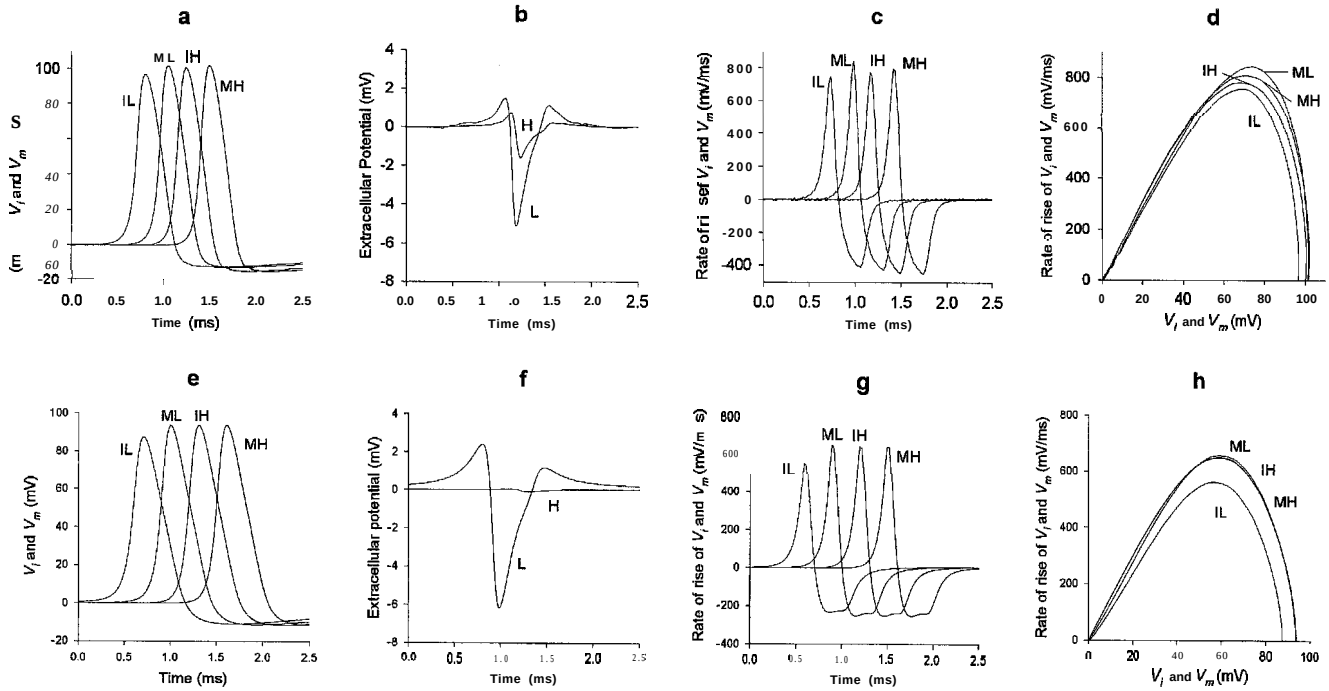

FIGURE 4 The waveforms of the intracellular and the membrane APs (*a* and *e*), the extracellular potentials (*b* and *f*), the rate of rise of APs (c and *g*), and the phase plots of the intracellular and the membrane APs (*d* and *h*). The upper panels ***(a-d)*** are recorded experimentally on the giant axon of a squid. The lower panels (*e–h*) are the results of simulation. L, H, I, and M stand for low ASW, high ASW, intracellular potential, and membrane potential. The high and low ASW levels provide the bath resistance of 108 Ω and 445 Ω, respectively, for the upper panel experimental results, and of 16 Ω and 1000 Ω for the lower panel simulation results. The values of the bath resistance in the simulation are selected to clearly demonstrate the differences between the low and the high ASWs, thus more extreme than the bath resistance in the experiments. Because of the low peak-to-peak amplitude of the extracellular potential (*f*) in the high ASW simulation resulted from using a low bath resistance (16 Ω), the high ASW simulation is similar to the expections of the classical l-D cable theory (Eq. 1) with a grounded extracellular space. The direct comparisons between the measurements and the simulations are in Fig. 7. The intracellular and the membrane potentials are relative to their resting states. The waveforms in ***a, c, e***, and *g* are separated horizontally for clarity.

DISCUSSION

To take advantage of the well-studied l-D theory (Eq. 1), many experiments in cardiac muscle were designed to reduce the dimension (Lieberman et al., 1975; Spach et al., 198 1,1987), by creating flat or near-flat wave fronts of propagation. In such cases, it was assumed that the l-D cable theory could be applied. Nonetheless, Spach et al. (198 1) found that there were contradictions between the observed behavior of the AP in the flat wave front propagation in cardiac muscle and the classical l-D cable theory. They observed a directional dependence, i.e., anisotropy, in the rising phases of their recorded intracellular AP and the transmembrane AP (derived from the difference between their intracellular and extracellular recordings) and also in the safety factor of propagation in the ventricular and the atria1 muscles of canine heart. Although the waveform of AP varies considerably between cells, at the tissue level the directional differences are significant (Spach et al., 1992; Spach and Heidlage, 1995). Compared to the propagation perpendicular to the muscle fibers (transverse propagation, TP), propagation along the fibers (longitudinal propagation, LP) is faster and associates with an intracellular AP with a lower maximum rate of depolarization, a larger time constant of the foot, a lower peak amplitude, a larger extracellular potential, and a lower safety factor of propagation. Such anisotropies can generate unidirectional block and reentry propagation in cardiac muscle (Spach et al., 198 1). The anisotropic propagation has been attributed either to the complex pattern of propagation created by the discontinuities in cardiac muscle (Spach et al., 1981; Spach, 1983), or to the current exchange between the surface and the depth fibers and the extracellular spatial current distribution (Wu et al., 1996), or to the two- or three-dimensional bidomain structure (Kootsey and Wu, 199 1; Pollard et al., 1992; Henriquez and Papazoglou, 1993; Henriquez et al., 1996; Roth, 1996). Although the above two- or three-dimensional bidomain simulation studies reproduced anisotropic propagation as observed experimentally, a theoretical insight was still needed. The quasi-l-D theory for cardiac muscle developed by Wu et al. (1996) extended the classical cable theory by including a component of the extracellular current representing the spatial distribution of the extracellular current and an intracellular coupling current representing the electrical connection between the surface and the depth fibers in cardiac muscle. Wu et al. showed that the effects of the extracellular bath current and the intercellular coupling current were equivalent to adding an additional membrane current, the virtual membrane current, and an extra mem-

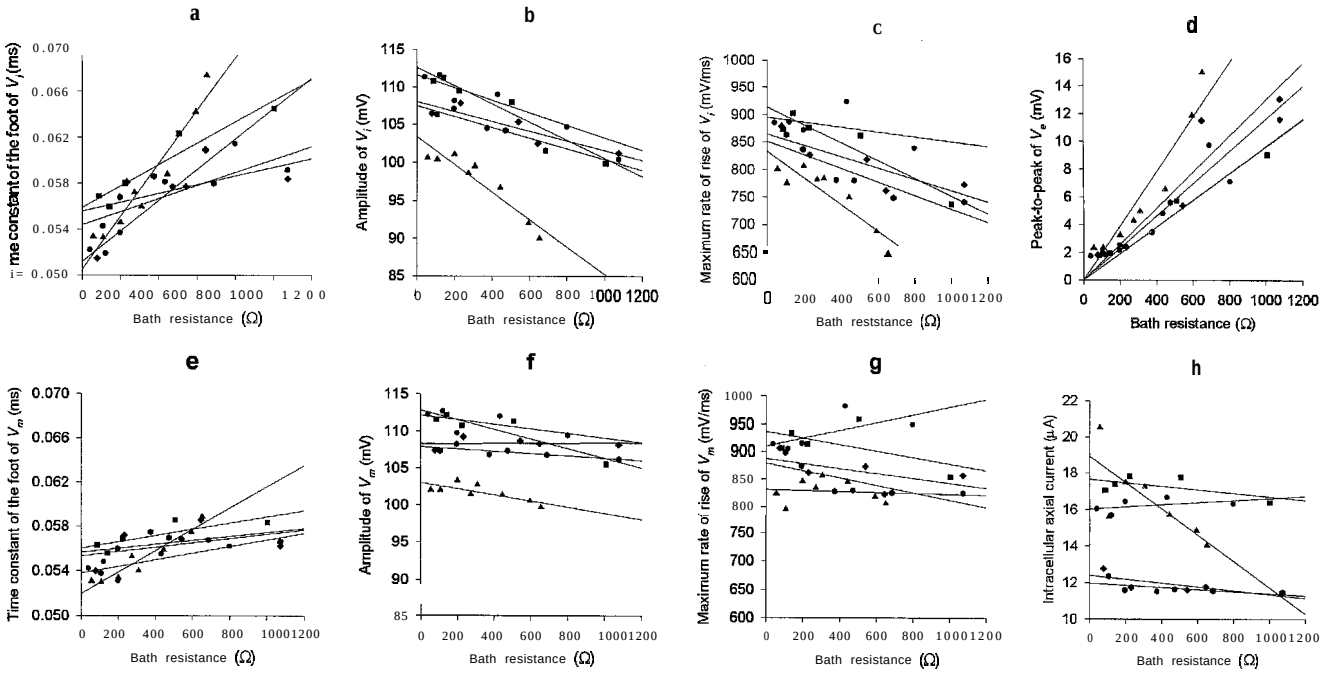

FIGURE 5 The effects of the bath resistance on the time constants of the foot of V_i *(a)* and V_{rm} *(e)*, on the amplitudes of V_i *(b)* and V_m *(f)*, on the maximum rates of rise of V_i *(c)* and V_m *(g)*, on the peak-to-peak amplitude of V_e *(d)* and on the intracellular axial current *(h)* of the data of five recording series from three squid giant axons. Each of the five different symbols (*square, triangle, circle*, etc.) corresponds to the data from a single set of recordings. The five lines in each plot are the least-squares for each set of data. The data points come from the averaged waveforms of 32 consecutive activations at the rate of 2/s in each recording.

brane capacitance, the virtual membrane capacitance, to the classical l-D cable model. The virtual membrane current and the virtual membrane capacitance modified the shape of the AP. They demonstrated with the equations and a simulation that the quasi- l-D theory could explain the anisotropic waveform of the action potential in cardiac muscle. In this paper, we further simplify the conditions required to produce a modified AP from the quasi-l-D theory.

This study demonstrates that when the classical l-D cable equation is modified to include the extracellular depth current, the observed relationships in the intracellular and extracellular potentials of the squid axon can be accounted for. Both the experiment and the simulation demonstrate that the quasi-l-D cable theory for squid axon can describe the effects of varied extracellular resistance more accurately than the classical l-D theory. As mentioned in the Introduction, the classical l -D theory does not expect any change in the waveforms of AP with the extracellular resistivity. With the addition of the extracellular depth current in the quasi-l -D cable theory, the classical l-D cable equation (Eq. 1) is extended to include a virtual membrane ionic current (Eq. 16). Therefore, the apparent membrane ionic current differs from the actual ionic current. This difference increases with the extracellular depth current. When a fiber is in oil ($i_d = 0$) or has a well-grounded extracellular space ($r_e = 0$), the virtual membrane ionic current does not exist. In these cases, the quasi-l-D cable model (Eq. 14) reverts to the classical l-D cable equation (Eq. 1). Since the quasi-l-D cable theory closely relates to the classic l-D cable theory, which is well studied and well understood, we write the quasi-l-D equation in a similar way. By introducing the virtual membrane current, we can rewrite the quasi-l-D

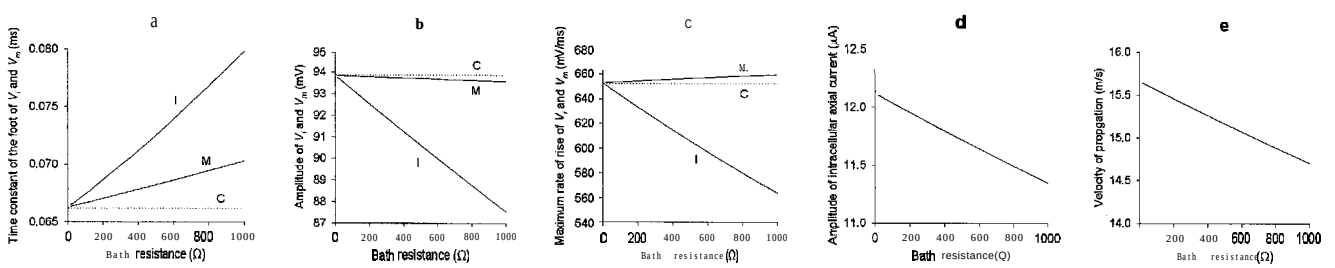

FIGURE 6 The effects of the bath resistance as determined by the simulation. I and M are the simulated intracellular and the membrane potentials of a quasi-l-D squid axon in bath. C is the predicted membrane potential from the classical l-D cable theory (Eq. 1).

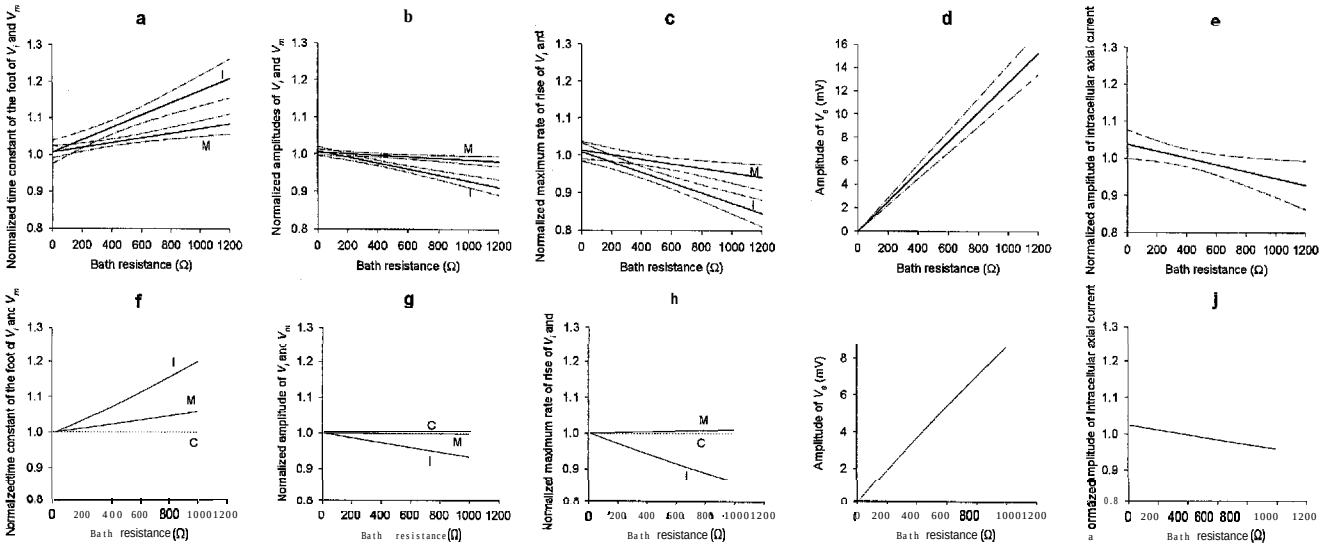

FIGURE 7 Comparison of the normalized (except *d* and *i*) and combined experimental results of the giant axons of the squid (*upper panels, a-e),* with the corresponding results of the simulations (*lower panels, f-j).* Plots *a-c* and *e* are derived from Fig. 5 by normalizing each set of data to the values with the lowest bath resistance *(a-c)* or to the averages of each set of data (e). In the same way, plots *f-h* and *j* are derived from Fig. 6. The thick lines in *a-e are* the least-square fittings of the combined normalized data from all five recording series. Each of the thick least-squares lines has 95% confidence limits indicated by a pair of thin dashed lines on both sides. I and M indicate the intracellular and the membrane potentials for the thick lines *(a-c)* and the solid lines *('f-h)* next to them, respectively. The dotted lines next to C in panels *f–h* are the membrane potentials predicted by the classical cable theory (Eq. 1).

cable equation in the form of the classical 1 -D core-conductor cable equation with the substitution of the membrane ionic current with the apparent membrane ionic current. In this way, the quasi-1-D equations are easier to understand and many analytical and mathematical analyses and methods developed for the l-D core-conductor cable can be readily adopted. It is also easier to see that the differences in the waveforms of APs result from the differences in the quasi-l-D equation and the classical 1 -D equation, i.e., are due to I_{vir}. As Eqs. 21 and 22 show, with the existence of i_d, the shapes of V_m, V_i, and V_e are no longer proportional, as in the classical l-D cable theory (Eq. 3). Such a result is more general and realistic. In view of the classical l-D cable equation, the apparent membrane ionic current affects the waveform of AP in a way similar to a membrane having a component of the membrane current that is related to the extracellular resistivity.

Our quasi-l-D theory for squid axon expects changes in both V_i and V_m, although changes in V_m are much smaller than in V_i. The V_i given by Eq. 13 and the V_m given by Eq. 19 are similar in form, except for their last terms on the right, i.e., the virtual membrane currents. Using the simulated V_e at the bath resistance per unit surface area of 625 Ω and the parameters in Table 1, we illustrate the virtual membrane currents for V_i (Eq. 13) and for V_m (Eq. 19) in Fig. 8. We include the membrane and the extracellular APs in Fig. 8 for comparing the timing of the virtual currents. Both the membrane ionic and the virtual currents start at the fast rising phase of the membrane AP, indicating the passiveness of the membrane at the foot of the AP. The amplitudes of the virtual currents for V_i and V_m are about one-tenth of the membrane ionic current, i_{ion}. Although the local membrane is passive at the time, the foot of AP is raised by the inflow current from the neighboring section, which is in the early stage of excitation and is affected by

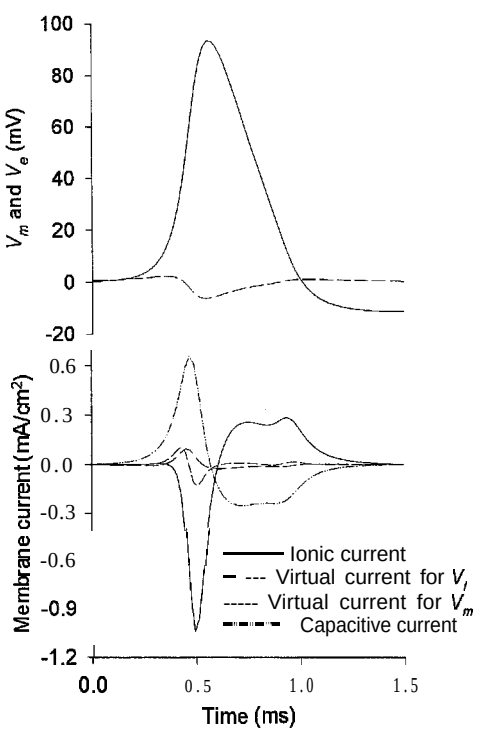

FIGURE 8 The membrane ionic current and the virtual membrane currents for V_i and V_m (*lower plot* and Eqs. 13 and 19) and the reference timing on V_m and V_e *(upper plot).* The data are the results of a simulation with a bath resistance of 653 Ω.

the virtual current there. The early virtual currents of both V_i and V_m are in the opposite direction of i_{ion} (see Fig. 8). Therefore, the inflow current, which is derived from the combined i_{ion} and the virtual current in the neighboring region and raises the foot of local AP, is reduced by the early virtual currents in the neighboring region. With a reduced inflow current, the time constant of the foot of local AP is increased. The fast rising phase of AP is powered by the local currents. The virtual current for V_i (Eq. 13) is monophasic and is in the opposite direction of i_{ion}. Thus, the virtual current for V_i reduces the total effective transmembrane electrical charge during the rising phase of the intracellular AP. The reduced total effective transmembrane electrical charge decreases the maximum rate of rise and the amplitude of the AP of V_i. However, as shown in Fig. 8, the virtual current for V_m (Eq. 19) is biphasic. Although the virtual currents for V_m and for V_i are similar at the early stage of excitation, the virtual current for V_m reversed direction around the time of the maximum membrane ionic current. Its overall contribution to the effective transmembrane electrical charge is smaller than the virtual current for V_i. Consequently, comparing to the modifications on the waveform of the intracellular AP by the virtual current for V_i, the corresponding modifications by the virtual current for V_m on the waveform of the membrane AP are smaller. The biggest effect of the bath resistance on the waveform of V_m is on the time constant of the foot.

The surface equivalent extracellular resistance per unit length of the fiber, r_e, and the extracellular equivalent depth resistance per unit axial length of the fiber at the surface, r_d, are abstract concepts representing the components of the extracellular resistance along and perpendicular to the fiber on the extracellular surface. They can be derived from the field theories for a fiber in an infinite or in a cylindrical medium. In case of cardiac muscle, their values depend on the size and the shape of the interstitial space, as well as the resistivity of the extracellular fluid. Thus, the values of r_e and r_d must be measured for cardiac muscle. We opted to describe the bath in detail in the simulation model of the propagation in the giant axon of squid, instead of the abstract extracellular space as in the quasi- l-D equations.

In contrast, Suenson (1985) demonstrated a separate mechanism of modifying the waveform of the AP. He showed that the waveform of the rising phase of the membrane AP (V_m) on the surface of the trabecula or papillary muscle (4– 8 mm long and 0.24–1 mm in diameter from ferret heart) changed as the volume of the surrounding Tyrode solution was restricted to a column centered at the muscle by a silicon bath. Therefore, he limited the extracellular current to the surface of membrane. In comparison with a large diameter of the bath column, a small diameter of the bath was associated with a membrane AP having a smaller time constant of the foot and a higher rate of rising and an extracellular potential with larger amplitude. He attributed the Tyrode volume-related changes in the waveform of AP to the wave front lag of the excitation in the middle of the muscle bundle. As he pointed out, the changes in the shape of action potential in his experiment were the result of the coupling between the surface and the depth cells. These differences between the observations of Suenson's and ours are the results of two separate mechanisms affecting the AP.

The version of the quasi-l-D theory for cardiac muscle and its simulation (Wu et al., 1996) contain both the extracellular spatial current as described by Eq. 20, and the coupling currents representing the electrical connection between the surface and the depth fibers. With the inclusion of the intracellular coupling current between the fibers, not only V_i and V_e, but also V_m are similar to Spach's observation. In that theory, the current coupling between the surface and the depth fibers produces a virtual membrane capacitance that is an extra term added to the physical membrane capacitance in the quasi-l-D cable equation. Hence, the effective membrane capacitance is modified. The effective membrane capacitance increases with the amplitude of the extracellular potential. In view of the quasi-l-D cable theory, our results on squid axon came from the modification of the effective membrane ionic current by the component of the extracellular current leaving the surface of the axon. Suenson's results came from the modification of the apparent membrane capacitance by the coupling current between the surface and the depth cells in the muscle bundle. A large Tyrode volume increased the wave front curvature in the muscle bundle and generated a large coupling current. Similar effects of modifying the apparent membrane capacitance were also demonstrated by Spach et al. (1987) on a simulated l-D monodomain cable by changing the membrane capacitance. Since the waveform modification occurs in squid axon, we suggest that neither three-dimensional structure nor discontinuities are required for the changes in waveforms in propagation, although both of them contribute to the anisotropic propagation in cardiac muscle substantially.

As shown in Table 2, the dependence of the changes in the shapes of V_i and V_e in an axon on bath resistance resembles the dependence of corresponding changes upon the direction of propagation in anisotropic cardiac muscle (Spach et al., 198 1). A high value of the time constant of the foot of V_i, τ_i, a high peak amplitude of V_i, a high maximum rate of rise of V_i, and a low peak-to-peak amplitude of V_e occur in cardiac muscle in transverse propagation and in the giant axon of squid with a high level of ASW. Similarly, both the longitudinal propagation in cardiac muscle and low ASW level 1 propagation in the squid giant axon showed the opposites: a low τ_i, a low peak V_i, a low maximum rate of rise of V_i, and a high peak-to-peak amplitude of V_e. Although both the waveforms for V_m n our simulation and that derived from our experimentally recorded V_i and V_e match very well with each other, they have smaller changes with different amplitude of the peak-to-peak amplitude of V_e than Spach's derived V_m. This difference in the V_m of squid axon and the V_m of cardiac muscle is caused by the absence of the coupling current in the giant squid axon as

TABLE 2 **The comparison of the changes in the action potentials of canine heart and the giant axon of squid**

	Peak-to-peak of V_e (mV)	Amplitude Of V_i (mV)	Maximum rate Of rise Of V_i (V/s)	Time constant of the foot of V_i (ms)	Amplitude of V_m (mV)	Maximum rate of rise of V_m (V/s)	Time constant of the foot of V_m (ms)
Canine ventricle* (velocity: 0.50 m/s LP, 0.19 m/s TP)							
LP	8.1	100	114	1.086	104	124	0.921
TP	6.2	106	155	0.681	110	171	0.669
TP/LP ratio	0.77	1.06	1.36	0.627	1.06	1.38	0.726
Canine atrium* (velocity: 1.0 m/s LP, 0.1 m/s TP)							
LP	7.0	111	144	0.375	112	161	0.375
TP	2.0	113	191	0.290	114	200	0.290
TP/LP ratio	0.29	1.02	1.33	0.773	1.02	1.24	0.773
Cardiac muscle' (simulation, velocity: 0.4566 m/s LP, 0.0535 m/s TP)							
LP	4.0258	77.7	105.1	0.494	79.0	115.8	0.443
TP	0.3760	80.91	125.1	0.376	81.0	126.1	0.370
TP/LP ratio	0.0934	1.04	1.19	0.761	1.03	1.09	0.835
Squid axon (simulation, bath resistance: 1000 Ω, Low ASW, 16 Ω High ASW)							
Low ASW	8.6	87.53	563.8	0.0798	93.58	659.6	0.0703
High ASW	0.15	93.75	651.5	0.0665	93.85	653.2	0.0663
High/Low ratio	0.017	1.07	1.17	0.833	1.00	0.99	0.943

*Experimental data from Table 1 in the paper by Spach et al. (1981).
'Simulation data from Table 1 and Fig. 4 in the paper by Wu et al. (1996)

existed between the surface and deeper cells in cardiac muscle, as we discussed above.

The extracellular depth current as defined in the quasi-l-D cable theory does exist in cardiac muscle. In a typical in vitro experiment (Spach et al., 1979, 1981), the preparation of cardiac tissue is immersed in the bathing solution. A reference electrode placed at a distant point in the bulk bathing solution, relative to the tissue preparation, is used to define zero potential. In a typical in vivo animal experiment, there are equivalent reference electrodes placed on the limbs of the animal. In both cases, the extracellular current is not constrained to the surface of cell, but is distributed though out the entire extracellular space. The observed biphasic extracellular potential (Spach et al., 1979) is the evidence of such extracellular "depth" current. Under such circumstances, the quasi-l-D cable equations developed in our previous study (Wu et al., 1996) and in the current one are preferable to the classical l-D equation (Eq. 1).

The field theories as we cited earlier are rigorous derivations for a uniform fiber in an infinite bath or in a cylindrical bath and are generally solved numerically. However, such geometrically simple and perfect baths are rare in biological systems. On the other extreme, the classical core conductor cable theory has no bath and often provides useful analytical insights. The quasi-l-D cable theory is in between the two extremes of either having an infinite bath or having no bath. It has a component of the extracellular current going into the bath, which is defined on the surface of the membrane as the sink or source to the surface current. Yet, the shape of the extracellular space is not defined (no infinite-bath or cylindrical-bath requirement). The quasi-l-D cable theory can be applied to any shape of the extracellular space, as long as it is uniform along the fiber. In this way, the quasi-l-D cable theory circumvents the problem of a geometrically simple and perfect extracellular space as required by the analytic field theories. The studies by Wu et al. (1996) and being presented here provide a quasi-l-D cable theory to achieve similar results as the field description with reduced computational complexity without the limitation of a particular geometry of the extracellular space. Therefore, the quasi-l-D theory is better suited for complicated extracellular space commonly seen in the biological tissue than the much more idealized field theories.

This study is complementary to the bidomain simulation models of cardiac muscle. Previously, bidomain models (Kootsey and Wu, 1991; Pollard et al., 1992; Henriquez and Papazoglou, 1993) reproduced some of the anisotropies in the action potential during the excitation propagation in cardiac muscle. The bidomain models had the advantage of being able to solve complex boundary conditions numerically and reproduce some sophisticated phenomena, e.g., the virtual electrode effects (Roth and Wikswo, 1996) in cardiac muscle. The analytical treatments by Wu et al. (1996) and the current study provide an intuitive explanation identifying a specific mechanism for the anisotropies in the action potential during the propagation in cardiac muscle, and clarify the contradictions between the experimental observation (Spach et al., 198 1) and the classical l-D cable theory.

The authors sincerely appreciate the help from our colleagues Shien-Fong Lin, Rashida Abbas, and Kevin Parker during our experiments on squid at the Marine Biological Laboratory at Woods Hole, MA. We are indebted to one of the anonymous reviewers for extensive comments that have greatly improved this manuscript. We also thank Bradley J. Roth for his comments and Margaret Khayat for her editorial assistance.

This work was supported by National Institutes of Health Grants HL46681 and HL52323.

REFERENCES

Adelman, Jr., W., and D. L. Gilbert. 1990. Electrophysiology and biophysics of the squid giant axon. *In* Squid as Experimental Animals. D. L. Gilbert, W. J. Adelman, Jr., and J. M. Arnold, editors. Plenum Press, New York. 117.

Andreassen, S., and A. Rosenfalck. 1981. Relationship of intracellular and extracellular action potentials of skeletal muscle fibers. *CRC Crit. Rev. Bioeng.* 6:267–306.

Clark, J., and R. Plonsey. 1966. A mathematical evaluation of the core conductor model. *Biophys. J.* 6:95–112.

Clark, J., and R. Plonsey. 1968. The extracellular potential field of the single active nerve fiber in a volume conductor. *Biophys. J.* 8:842–864.

Eisenberg, R. S., V. Barcilon, and R. T. Mathias. 1979. Electrical properties of spherical syncytia. *Biophys. J.* 25:151–180.

Henriquez, C. S., A. L. Muzikant, and C. K. Smoak. 1996. Anisotropy, fiber curvature, and bath loading effects on activation in thin and thick cardiac tissue preparations: simulations in a three-dimensional bidomain model. *J Cardiovasc Electrophysiol.* 7:424–444.

Henriquez, C. S., and A. A. Papazoglou. 1993. Conduction in a 3D bidomain representation of cardiac tissue with unequal anisotropy ratios. *Proc. Annu. Int. Conf. IEEE EMBS.* 15:758–759.

Henriquez, C. S., and R. Plonsey. 1990. Simulation of propagation along a cylindrical bundle of cardiac tissue I: mathematical formulation. *IEEE Trans. Biomed. Eng.* 37:850–860.

Henriquez, C. S., N. Trayanova, and R. Plonsey. 1988. Potential and current distributions in a cylindrical bundle of cardiac tissue. *Biophys. J.* 53:907–918.

Hodgkin, A. L. 1954. A note on conduction velocity. *J. Physiol.* 125: 221–224.

Hodgkin, A. L., and A. F. Huxley. 1952. A quantitative description of membrane current and its application to conduction and excitation in nerve. *J. Physiol.* 117:500–544.

Hodgkin, A. L., and B. Katz. 1949. The effect of sodium ions on the electrical activity of the giant axon of the squid. *J. Physiol. (Lond.).* 108:37–77.

Kelvin, Lord William Thomson. 1855. On the theory of the electric telegraph. *Proc. R. Soc. (Lond.).* 7:382–390.

Kootsey, J. M., and J. Wu. 1991. Models of electrophysiological activation. Imaging, Measurement and Analysis of the Heart. S. Sideman and R. Beyar, editors. Hemisphere Publishing Corporation, New York. 373–381.

Leon, L. J., and F. A. Roberge. 1990. A new cable model formulation based on Green's theorem. *Ann. Biomed. Eng.* 18:1–17.

Leon, L. J., and F. A. Roberge. 1991. Structure complexity effects on transverse propagation in a two-dimensional model of myocardium. *IEEE Trans. Biomed. Eng.* 38:997–1009.

Lieberman, M., T. Swanobori, J. M. Kootsey, and E. A. Johnson. 1975. A synthetic strand of cardiac muscle: its passive electrical properties. *J. Gen. Physiol.* 65:527–550.

Plonsey, R. 1974. The active fiber in a volume conductor. *IEEE Trans. Biomed. Eng.* BME-21:371–381.

Plonsey, R., and R. C. Barr. 1988. *Bioelectricity.* Plenum Press, New York. 305 pp.

Pollard, A. E., N. Hooke, and C. S. Henriquez. 1992. Cardiac propagation simulation. *Crit. Rev. Biomed. Eng.* 20:171–210.

Roth, B. J. 1996. Effects of a perfusing bath on the rate of rise of an action potential propagating through a slab of cardiac tissue. *Ann. Biomed. Eng.* 24:639–646.

Roth, B. J., and J. P. Wikswo, Jr. 1996. The effect of externally applied electrical fields on myocardial tissue. *Proc. IEEE.* 84:379–391.

Rudy, Y., and W. Quan. 1987. A model study of the effects of the discrete cellular structure on electrical propagation in cardiac tissue. *Circ. Res.* 61:815–823.

Shiba, H. 1971. Heaviside's "Bessel cable" as an electric model for flat simple epithelial cells with low resistive junctional membranes. *J. Theoret. Biol.* 30:59–68.

Shiba, H., and Y. Kanno. 1971. Further study of the two-dimensional cable theory: an electric model for flat thin association of cells with a directional intercellular communication. *Biophysik.* 7:295–301.

Spach, M. S. 1983. The discontinuous nature of electrical propagation in cardiac muscle. *Ann. Biomed. Eng.* 11:209–261.

Spach, M. S., P. C. Dolber, J. F. Heidlage, J. M. Kootsey, and E. A. Johnson. 1987. Propagating depolarization in anisotropic human and canine cardiac muscle: apparent directional differences in membrane capacitance. A simplified model for selective directional effects of modifying the sodium conductance on $\dot{V}_{max}$, τ_{foot}, and the propagation safety factor. *Circ. Res.* 60:206–219.

Spach, M. S., and J. F. Heidlage. 1995. The stochastic nature of cardiac propagation at a microscopic level. Electrical description of myocardial architecture and its application to conduction. *Circ. Res.* 76:366–380.

Spach, M. S., J. F. Heidlage, E. R. Darken, E. Hofer, K. H. Raines, and C. F. Starmer. 1992. Cellular V_{max} reflects both membrane properties and the load presented by adjoining cells. *Am. J. Physiol.* 263: H1855–H1863.

Spach, M. S., W. T. Miller, D. B. Geselowitz, R. C. Barr, J. M. Kootsey, and E. A. Johnson. 1981. The discontinuous nature of propagation in normal canine cardiac muscle. Evidence for recurrent discontinuities of intracellular resistance that affect the membrane currents. *Circ. Res.* 48:39–54.

Spach, M. S., W. T. Miller, E. Miller-Jones, R. B. Warren, and R. C. Barr. 1979. Extracellular potentials related to intracellular APs during impulse conduction in anisotropic canine cardiac muscle. *Circ. Res.* 45:188–204.

Suenson, M. 1985. Interaction between ventricular cells during the early part of excitation in the ferret heart. *Acta Physiol. Scand.* 125:81–90.

Trayanova, N., and C. S. Henriquez. 1991. Modification of a cylindrical bidomain model for cardiac muscle. *Mathematical Biosciences.* 104: 59–72.

Trayanova, N., C. S. Henriquez, and R. Plonsey. 1990a. Extracellular potential and currents of a single active fiber in a restricted volume conductor. *Ann. Biomed. Eng.* 18:219–238.

Trayanova, N., C. S. Henriquez, and R. Plonsey. 1990b. Limitations of approximate solutions for computing the extracellular potential of single fibers and bundle equivalents. *IEEE Trans. Biomed. Eng.* 37:22–35.

Tung, L. 1979. Three-dimensional cable theory: a bi-domain model. *Biophys. J.* 25:214*a* (Abstr.).

van Egeraat, J. M., and J. P. Wikswo, Jr. 1993. A model for axonal propagation incorporating both radial and axial ionic transport. *Biophys. J.* 64:1287–1298.

Wikswo, J. P., Jr., and J. M. van Egeraat. 1991. Cellular magnetic fields: fundamental and applied measurements on nerve axons, peripheral nerve bundles, and skeletal muscle. *J. Clin. Neurophysiol.* 8:170–188.

Wikswo, J. P., Jr., P. C. Samson, and R. P. Giffard. 1983. A low-noise low input impedance amplifier for magnetic measurements of nerve action currents. *IEEE Trans. Biomed. Eng.* 30:215–221.

Wu, J., E. A. Johnson, and J. M. Kootsey. 1996. A quasi-one-dimensional theory for anisotropic propagation of excitation in cardiac muscle. *Biophys. J.* 71:2427–2439.